Chinese Journal of Chemical Engineering 55 (2023) 111–122

Contents lists available at ScienceDirect

Chinese Journal of Chemical Engineering

journal homepage: www.elsevier.com/locate/CJChE

Full Length Article

Study on cavern evolution and performance of three mixers in agitation of yield-pseudoplastic fluids

Songsong Wang [1], Hong Li [2], Changyuan Tao [1,3], Renlong Liu [1,3], Yundong Wang [4], Zuohua Liu [1,3,*]

[1] *School of Chemistry and Chemical Engineering, Chongqing University, Chongqing 400044, China*
[2] *Graduate School, Chongqing University, Chongqing 400044, China*
[3] *State Key Laboratory of Coal Mine Disaster Dynamics and Control, Chongqing 400044, China*
[4] *Department of Chemical Engineering, Tsinghua University, Beijing 100084, China*

ARTICLE INFO

Article history:
Received 25 March 2022
Received in revised form 31 May 2022
Accepted 2 June 2022
Available online 10 June 2022

Keywords:
Cavern
Apparent viscosity
Mixing
Yield-pseudoplastic fluids
Computational fluid dynamics (CFD)

ABSTRACT

The hydrodynamic performance of three mixers (single shaft central mixer (SSC), single shaft off-centred mixer (SSO), dual shaft off-centred mixer (DSO), was investigated in the mixing of yield-pseudoplastic fluids (xanthan gum solutions) in the laminar regime. To explore and determine the efficiency of three mixers, both numerical and experimental approaches were adopted. The fluid rheology was described by the Herschel–Bulkley rheological model. Computational fluid dynamics was employed to simulate the apparent viscosity distribution, mixing time, and the flow pattern inside the stirred tank. The developed model was validated through experimentally measured torque. The influence mechanism of the rotational speed and fluid rheology on the cavern evolution was explored deeply. The performances of three mixers in this work were compared at the constant power input and fluid rheology with respect to the flow pattern, mixing time, and mixing efficiency. The results verify that the faster the rotating speed, the greater influence of the fluid rheology on the cavern evolution, and the more uniform apparent viscosity distribution. Moreover, the mixing time decreases continuously as the increasing power consumption per unit volume, and the dimensionless mixing time of DSO mixer was nearly 42.8% and 6.1% shorter than that of SSC and SCO mixer at the same Reynolds number, respectively. According to the mixing efficiency criteria, these data also revealed that DSO was more efficient than SSC and SSO.

1. Introduction

The mixing of pseudoplastic fluid gradually become vital with the development of modern chemical industry, which is extensively applied in many industries such as polymer, food, biotechnology and cosmetics. The viscosity of pseudoplastic fluid is non-uniformly distributed in different regions of stirred tank, which leads to unique mixing performance [1–3], and a series of problems, such as gel formation, wall fouling, and accumulation, low heat transfer, and high mixing time, forming well-mixed region close to impeller (called cavern) with dead or stagnant zones in the rest of the tank [4–9]. Therefore, it is particularly significant to predict the evolution law of cavern, and eliminate cavern phenomenon by obtaining the overall mixing of pseudoplastic fluids.

The scholars carried out much research on the characteristics of cavern [10–15]. Different mathematical models were proposed to predict cavern development. The classical models mainly included the spherical model [16], cylindrical model [17], and torus model [18]. It revealed that the cylindrical model was more suitable to describe cavern characteristics than other models, while the spherical model overestimated the size of cavern, and the torus model might predict better the shape of the pseudo-cavern in mixing the power-law fluids [19,20]. Hence, Wilkens *et al.* [21] and Xiao *et al.* [22] established the elliptical torus model and apple torus model respectively to better describe the size and shape of caverns.

In terms of optimizing and designing the mixing system, many scholars were engaged in related research on the mixing of highly viscous fluids. Luan *et al.* [23] dislocated the blades of the six-bent-blade (6BT) impeller up and down, named it the impeller of perturbed six-bent-bladed turbine (6PBT), and compared the mixing performance of stirred pseudoplastic fluids with the 6BT impeller. The results demonstrated that the 6PBT impeller had stronger chaotic characteristics in mixing pseudoplastic fluid under the same working condition. Liu *et al.* [24] used a rigid-flexible impeller to explore the chaotic mixing characteristics of high-viscosity

* Corresponding author.
E-mail address: liuzuohua@cqu.edu.cn (Z. Liu).

https://doi.org/10.1016/j.cjche.2022.06.001
1004-9541/

stirred fluids. The results showed that the rigid-flexible paddle could improve the largest Lyapunov exponents (LLE) of the system by about 10.29% compared with the traditional rigid impeller. Gu *et al.* [25] explored the laminar mixing characteristics of non-Newtonian CMC solutions in a stirred tank, and found that the dimensionless mixing time for punched rigid-flexible impeller was shorter than that for rigid impeller and rigid-flexible impeller at the same power consumption per unit volume (P_v). Aubin *et al.* [26] investigated the mixing characteristics of multi-layer impellers for high-viscosity fluids by computational fluid dynamics (CFD). They concluded that the distance of the lower two impellers was slightly reduced to ensure that the fluid could exchange between the impellers when the Reynolds number (*Re*) was less than 27. Pakzad *et al.* [27–29] used a concentric double-shaft stirred tank to carry out related research on the mixing characteristics of non-Newtonian fluids. The results showed that the concentric double-shaft stirred tank was more conducive to the mixing of non-Newtonian fluids compared with traditional stirred tank. Gabriel *et al.* [30] measured the mixing time based on the color-changing technology of rapid acid-base reaction. They found that the dual off-centered impellers were more likely to destroy the separation area, and shorten the mixing time compared with the single-center impeller. Cabaret *et al.* [31] investigated the hydrodynamic properties of high viscosity Newtonian fluids by dual off-centered impellers. The results suggested that dual off-centered shaft mixer was more energy efficient than single shaft mixer, and the mixing time of the counter-rotating impeller was shorter than that of the co-rotating impeller in the stirred tank with dual off-centered impellers.

It is clear from the above studies that unconventional mixing strategies appear to reduce the mixing time in stirred tanks under laminar flow and transition regime conditions. A thorough search in the literature suggests that limited effort has been devoted to the study of non-Newtonian fluid flows in a stirred tank with different impeller arrangements. Therefore, the focus of the present study was to investigate cavern evolution of the xanthan gum solution and its mixing characteristics in stirred tanks with three impeller arrangements (single shaft central mixer, single shaft off-centred mixer, dual shaft off-centred mixer, *i.e.* single shaft central mixer (SSC), single shaft off-centred mixer (SSO), dual shaft off-centred mixer (DSO)). Three-dimensional numerical simulations of the flow fields generated by the stirred tanks were carried out by CFD. This study provides an exciting opportunity to advance our knowledge of the cavern evolution of pseudoplastic fluids and the arrangement of impellers in a stirred tank.

2. Experimental Set-up, Materials and Strategy

2.1. Experimental set-up

The structure of the cylindrical flat-bottomed stirred tank (diameter is $T = 240$ mm) with three impeller arrangements, as shown in Fig. 1. Four equally spaced baffles (width: $w = T/10$) were fitted in the tank, the clearance from baffle to the tank wall was 2 mm, and each shaft was equipped with a rotary torque sensor with two flexible couplings to continuously measure the torque. For four monitoring points, P_1, P_2, P_3 and P_4, their distances from the wall were all 20 mm, the clearance of P_1 and P_2 from the off-bottom was 40 and 160 mm, respectively. The off-bottom clearance was 300 mm for P_3 and P_4, P is the feed point of the tracer. As depicted in Fig. 2, the impellers used in experiment were Rushton turbine impellers (diameter is $D = T/3$), and the total height of liquid in the tank was 500 mm. All of the blade thicknesses were 2 mm. In addition, the dimensions of various parts are given in Table 1.

Taking the single shaft stirred experiment as an example, the experimental setup is shown in Fig. 3. The main devices include

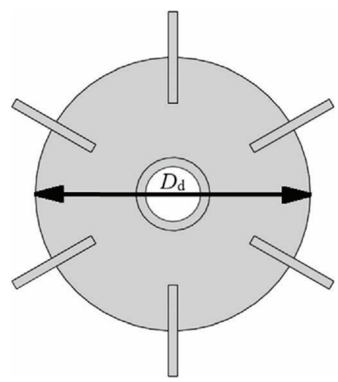

Fig. 2. Structure diagram of the Rushton impeller.

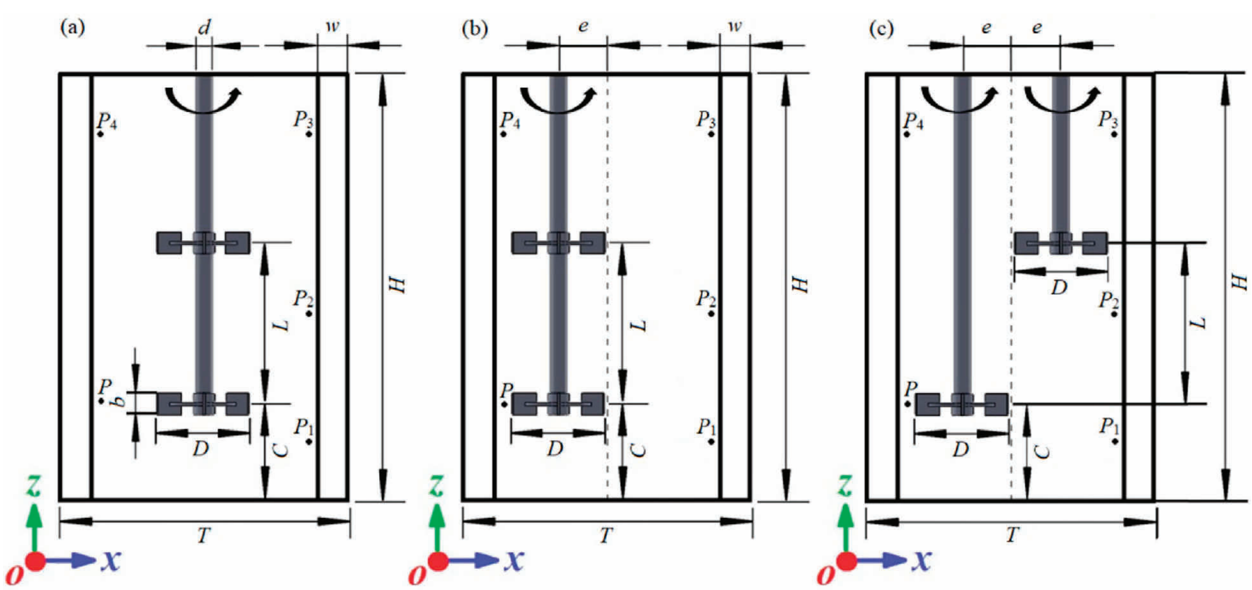

Fig. 1. Diagrams of the stirred tank with three impeller arrangements: (a) SSC, (b) SSO, (c) DSO.

Table 1
Dimensions of various parts in the stirred tank

T/mm	b/T	C/T	d/T	D_d/T	e/T	L/T
240	0.067	0.333	0.058	0.25	0.167	0.5

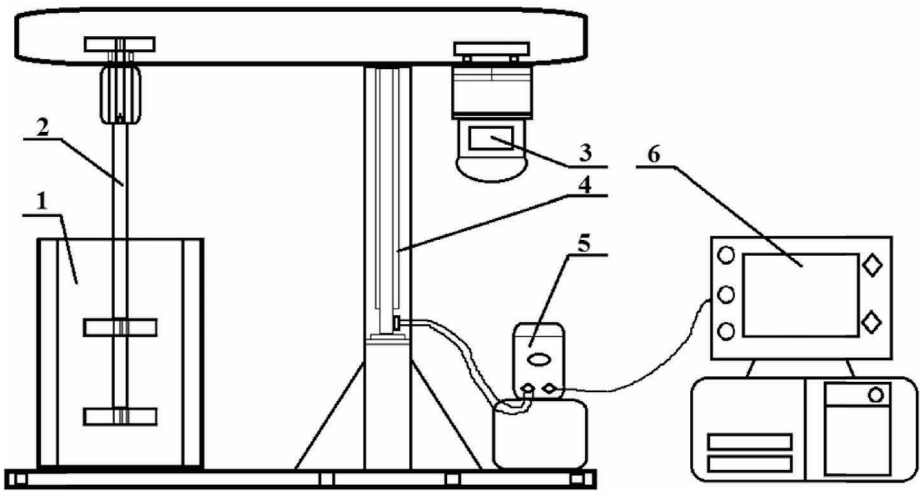

Fig. 3. Schematic diagram of stirred experimental system: 1—stirred tank; 2—stirred shaft; 3—electromagnetic speed regulating motor; 4—hydraulic lifting frame; 5—hydraulic pump; 6—data collection system.

the lifting frame, stirred equipment, electromagnetic speed regulating motor, and data collection system.

2.2. Materials and strategy

The xanthan gum solutions were used as the working medium at concentrations ranging from 1.2% to 1.8%. The mass fraction, densities, and rheological parameters of the xanthan gum solutions applied in this study are listed in Table 2 [15].

The rheology of xanthan gum solution is by the Herschel–Bulkley model [32,33], which can be expressed as:

$$\tau = \tau_y + K\dot{\gamma}^n \tag{1}$$

where $\dot{\gamma}$ is the shear rate.

The average shear rate $\gamma_{\rm avg}$ can be calculated by the Metzner and Otto's method [34]:

$$\gamma_{\rm avg} = k_{\rm s}N \tag{2}$$

For radial flow impeller, $k_{\rm s}$ = 11.5 [35].

The apparent viscosity $\eta_{\rm a}$ of the solution and the apparent Reynolds number Re^* can be defined as, respectively:

$$\eta_{\rm a} = \frac{\tau}{\gamma_{\rm avg}} = \frac{\tau}{k_{\rm s}N} = \frac{\tau_{\rm y} + K(k_{\rm s}N)^n}{k_{\rm s}N} \tag{3}$$

$$Re^* = \frac{k_{\rm s}N^2D^2\rho}{\tau_{\rm y} + K(k_{\rm s}N)^n} \tag{4}$$

3. Numerical Methodology

3.1. Computational model

The rotational speed was set between 120 to 660 r·min^{-1} in CFD calculation, and the corresponding Reynolds numbers (Re^*) range from 4.5 to 203.4. The laminar flow model was employed to simulate the mixing of xanthan gum solution in a stirred tank [12,27,28]. The fluid domain was discretized with tetrahedral mesh by the software Fluent 2020 customized. The whole solution domain was divided into three zones, two inner rotating zones enclosing the inner two impellers, and the inner static zone of the rest of the stirred tank.

Meanwhile, the zones near the impeller and wall are refined owing to the large velocity gradient. The meshing results of the three mixers are shown in Fig. 4. The original 3D mesh had about 342800 cells. To verify the grid independence [27,33,36], the number of cells was increased to about 537200 and 786900, respectively. These increases changed the velocity and power number in rotor region by more than 3%. Finally, the number of cells was further increased to 1103168, the power number and velocity changed by less than 3%. Therefore, the mesh sizes of the rotating and stationary domains were finally determined to be 2 and 4 mm, respectively, and 1103168 cells were employed in numerical simulations.

The multiple reference frame (MRF) method was adopted to simulate the rotation of the impeller [37,38]. This technique has been found to make flow field predictions comparable to those

Table 2
The rheological parameter of xanthan gum solution at different mass fractions

Mass fraction, w_t/%	Yield stress, τ_y /Pa	Consistency coefficient, K/Pa·s^n	Density, ρ/kg·m^{-3}	Rheological index, n	Yield viscosity, η_y
1.2	4.38	8.70	991	0.31	25.8
1.4	7.17	11.67	990	0.28	46.1
1.6	9.46	19.55	988	0.26	63.5
1.8	11.49	23.92	986	0.25	81.3

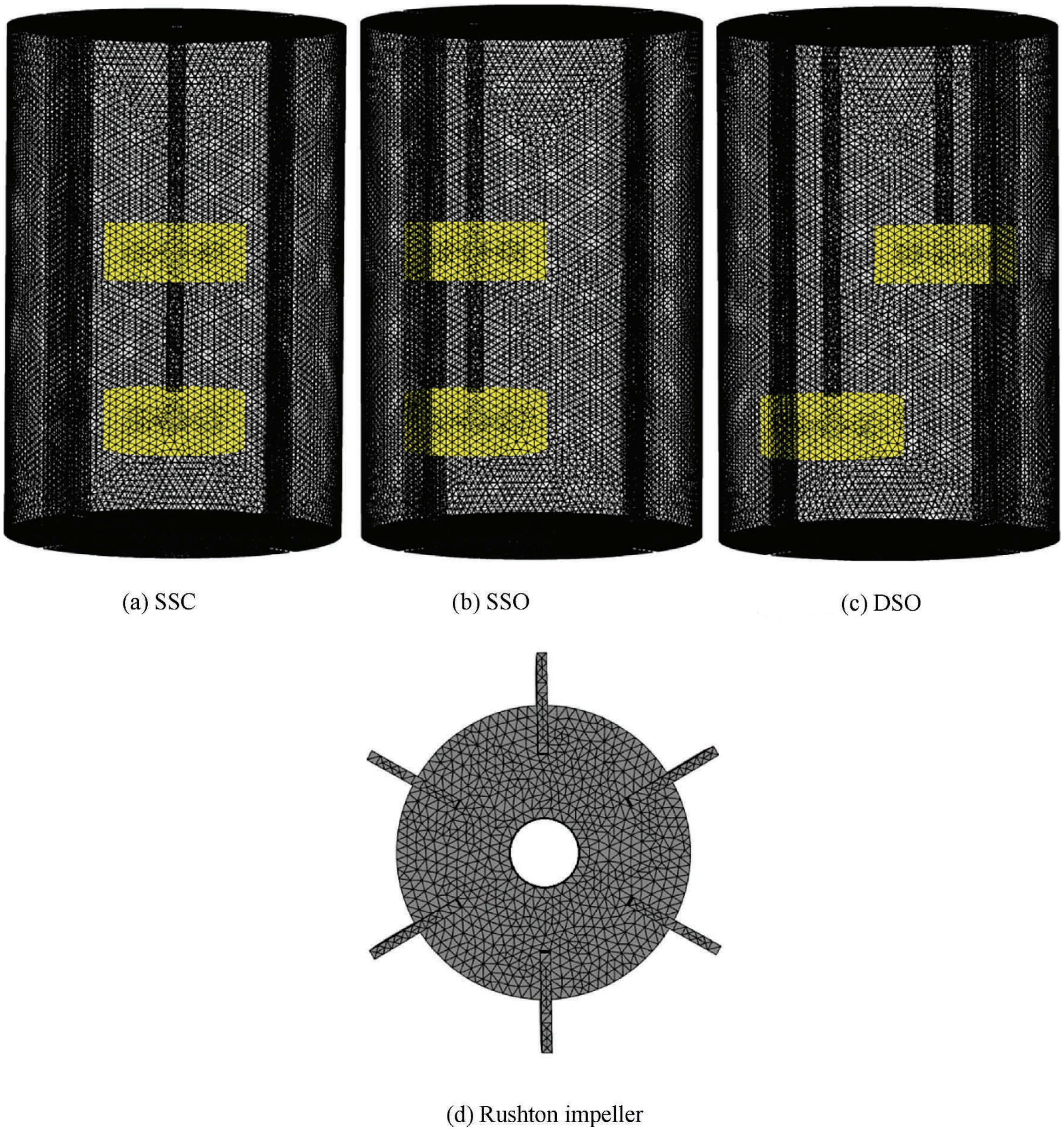

Fig. 4. Computational grids of three stirred tanks.

obtained using the sliding mesh (SM) approach, and meantime, the MRF method can reduce computational requirements [39,40]. The coincident surfaces between the rotor zone and stator zone were set as "Interface". No-slip boundary condition ($V = 0$) was assumed on the tank wall, bottom and shaft. The top surface was modeled as "symmetric" boundary. The second-order upwind discretization scheme was adopted to calculate the momentum equations. Pressure–velocity coupling was performed by SIMPLE algorithm [28,41]. The 3D coordinate origin was chosen at the center of the impeller, with the z-axis pointing towards the liquid surface and the stirrer rotating around the z-axis in a counterclockwise direction. The calculated results were considered converged when the scaled residuals for each transport equation were below 1×10^{-5}. The original data of all velocities were set as 0.

3.2. Validation of computational model

The power consumption P can be solved by using Eq. (5).

$$P = 2\pi NM \tag{5}$$

where N is the speed, and M is the torque of the shaft and impeller, which can be obtained by torque test and numerical calculation.

The power consumption experiment of xanthan gum solution with mass fraction of 1.2%, was carried out to verify the simulated results. Experimental data of power consumption at different speeds were compared to CFD calculated values, as indicated in Fig. 5. It found that the experimental data and simulation values were always in good agreement at different stirred speeds, and the maximum deviation was only 8.6%, which verified the laminar viscous model established in this paper and indicated that the CFD results were reliable.

4. Results and Discussion

4.1. Effect of stirred speed

Based on yield viscosity method, Luan *et al.* [15] defined the cavern boundary of pseudoplastic fluid flow field. The results showed that compared with the velocity method, the yield viscos-

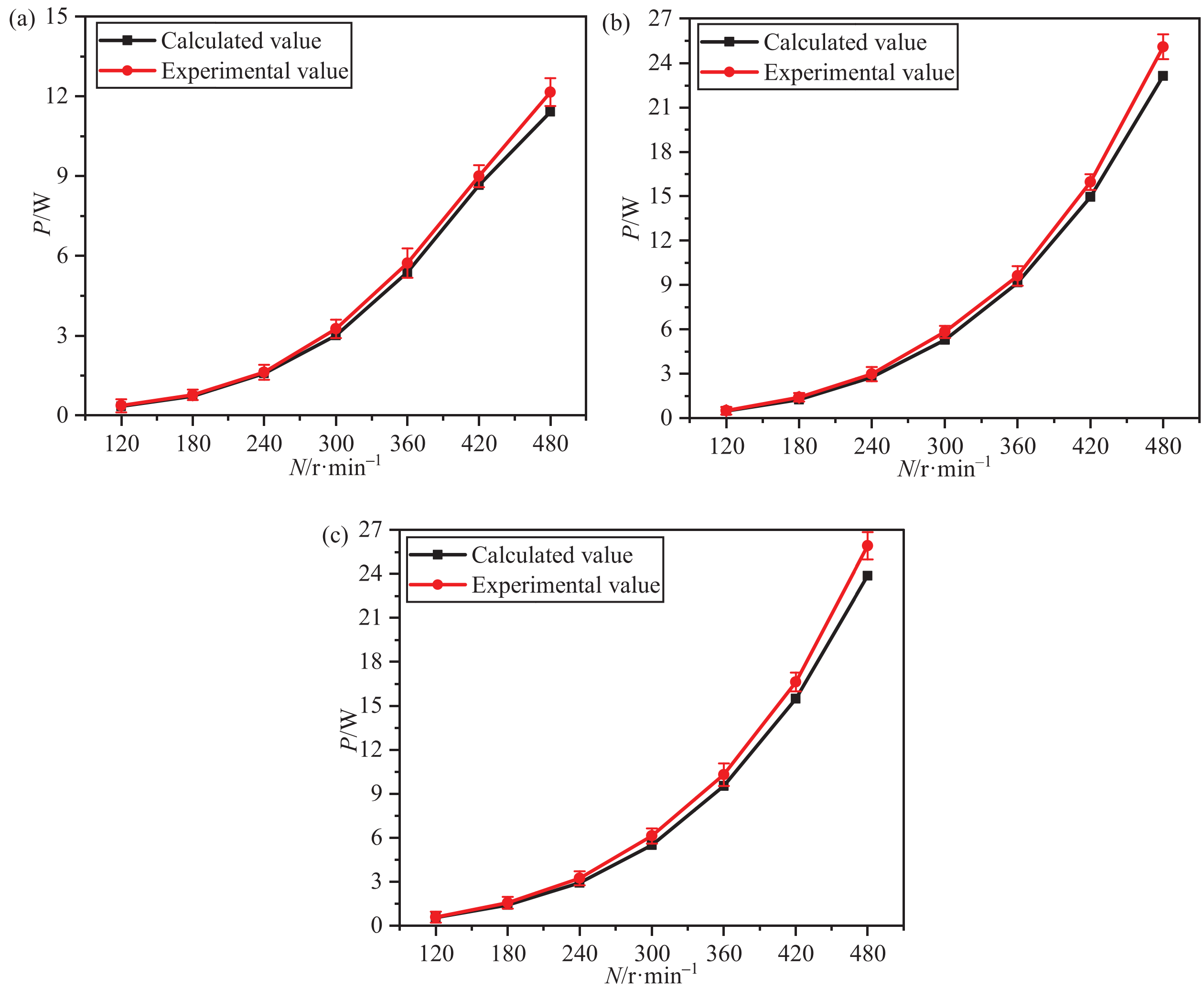

Fig. 5. Comparison of CFD and experimental power values at different speeds: (a) SSC, (b) SSO, (c) DSO.

ity method can maintain its accuracy all the time free from the influence of the impeller speed. Therefore, the yield viscosity method was employed to describe the cavern boundary in this work.

The apparent viscosity contours of xanthan gum solution (w_t = 1.2%) at different stirred speeds obtained by CFD simulation, as shown in Fig. 6. There are obvious flow dead zones (red zone) in three mixers at low speed (180 r·min^{-1}). Although the cavern area of the three mixers becomes larger as the speed increases from 180 to 420 r·min^{-1}, the stagnant or slow-moving fluid areas still existed in the stirred tank, which indicated that the cavern phenomenon has not been fully eliminated. Fortunately, under the same stirring condition, the cavern distribution area generated by DSO mixer is always greater than that by SSC and SSO, which testify that the advantages of DSO in terms of eliminating the cavern phenomenon.

To quantify the variations of apparent viscosity distribution created by three mixers, the original apparent viscosity distribution was carried out with Image Pro Plus 6.0 software. Fig. 7 shows the binary image of black and white with a width of 477 pixels and a height of 715 pixels, where the white area is η > 6.55 Pa·s area, black area (cavern area) is $\eta \le 6.55$ Pa·s area.

Through the calculation of Eq. (6), the ratio of the black area to the total area was achieved at different stirred speeds.

$$A_{\text{ratio}} = \frac{A_{\eta \le 6.55\ \text{Pa·s}}}{A_{\text{total}}} \tag{6}$$

The A_{ratio} of three agitators at different stirred speeds is demonstrated in Fig. 8. The value of A_{ratio} increases as the increase of impeller speed (120–480 r·min^{-1}), whereas the variation of the curve is close to smooth with further increase of the speed (480–660 r·min^{-1}). When the curve changes from an oblique line to a horizontal straight line nearly, which means that the volume of cavern has reached a stable value, that is, the maximum value. In addition, under the same working conditions, the A_{ratio} values of DSO mixer are always greater than that of SSC and SSO mixer, which shows the advantages of DSO mixer in stirring pseudoplastic fluid mixing.

4.2. Effect of fluid rheology

Fig. 9 shows the A_{ratio} variations of xanthan gum solutions with different mass fractions at different speeds stirred by SSC, SSO and DSO, respectively. The fluid rheology has little influence on the variation of A_{ratio} at the low speed (N = 120 r·min^{-1}), the corresponding maximum absolute value of slope is 0.05. As the speed increases to 300 r·min^{-1}, the A_{ratio} shows a downward trend with the increase of the fluid mass fraction, and there is a greater decrease with the further increase of speed range from 480 to 660 r·min^{-1}. When the area of cavern approached or reached its stable value, that is, the corresponding speed is 660 r·min^{-1}, the variation range of the cavern area has the most obvious trend of

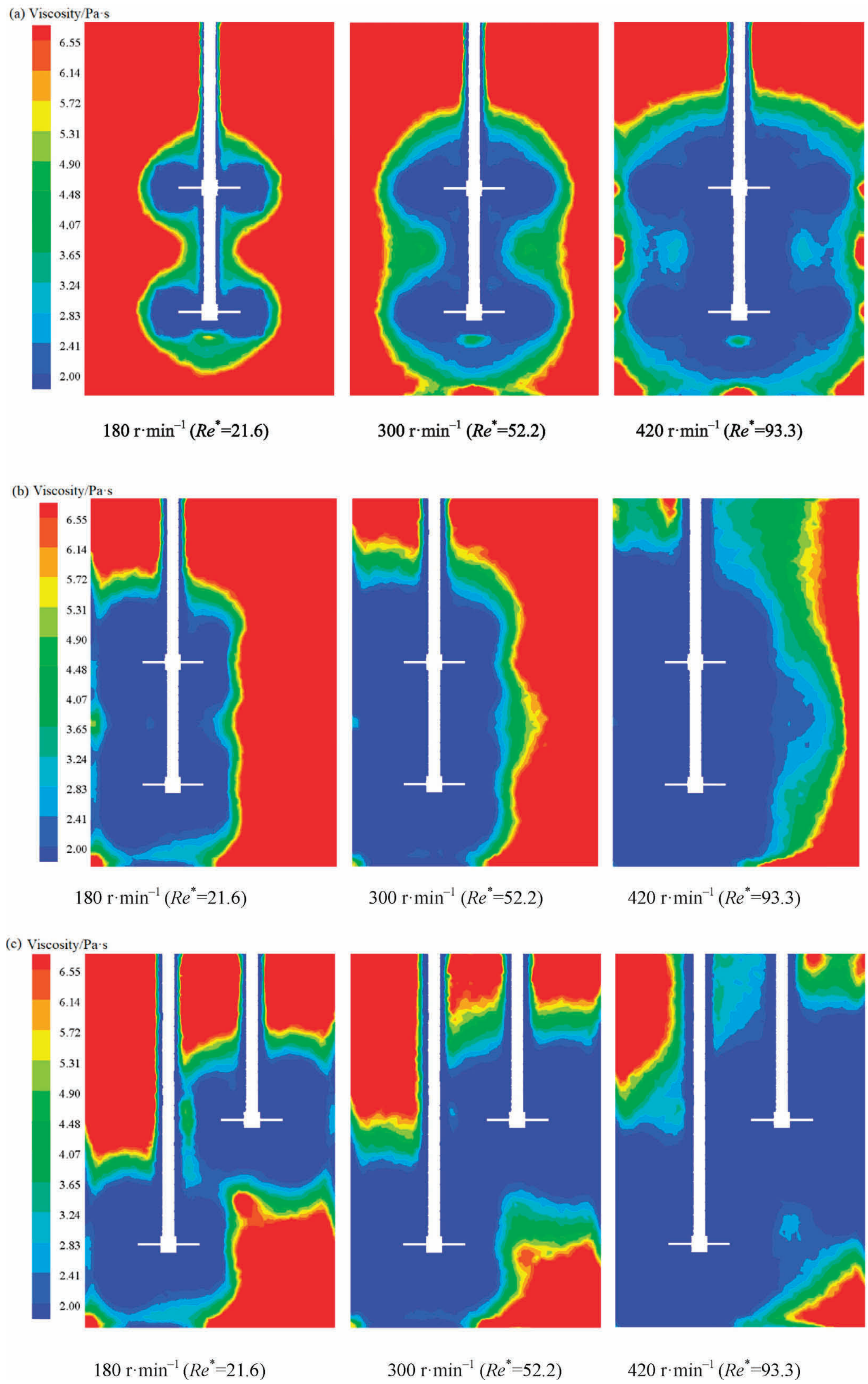

Fig. 6. The apparent viscosity cloud diagram for three mixers at different stirred speeds: (a) SSC, (b) SSO, (c) DSO.

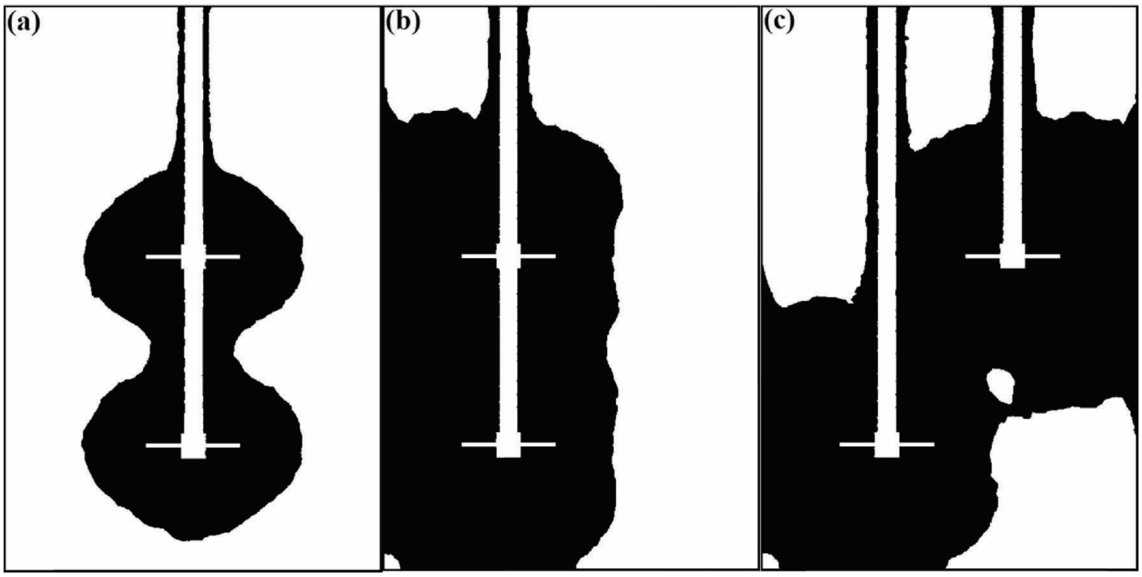

Fig. 7. Post-processing image of apparent viscosity for three mixers at 180 r·min^{-1}: (a) SSC, (b) SSO, (c) DSO.

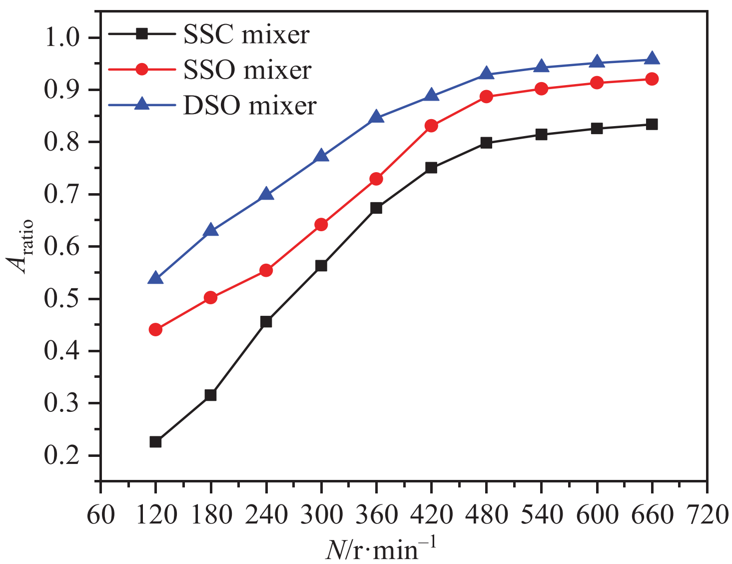

Fig. 8. The A_{ratio} of three mixers in the axial lengthwise section at different speeds.

decreasing as the increase of the mass fraction, and the maximum absolute value of the corresponding slope is up to 0.31.

The flow range of fluids decreased with the increase of yield stress, which results in a change in the cavern area. Moreover, it is also observed that the A_{ratio} generated by DSO is always higher than that by SSC and SSO, which indicates that dual shaft off-centred impellers are more conductive in eliminating the cavern phenomenon of pseudoplastic fluids in a stirred tank.

As shown in Fig. 10, the variation curves of the absolute value of slope for three mixers at different speeds. The slope corresponding to the A_{ratio} values of different mass fractions has a linear relationship with the rotational speeds. The results showed that the faster the rotating speed, the greater influence of fluid rheology on cavern area.

4.3. Flow pattern

The mixing performance of a stirred system is affected by the flow pattern, which depends on the factors such as the number of impellers, impeller spacing, arrangement of the impellers, and rheology of the fluid. The focus of this section is to evaluate numerically, the mixing performances of the three mixers by comparing the flow pattern generated inside the stirred tanks at the fixed power consumption.

In order to analyze and explore the flow field generated inside the stirred tank, the velocity contour plots of three stirred tanks, were obtained from the CFD model for the vertical planes as illustrated in Fig. 11. It can be noticed in Fig. 11(a) that the use of the SSC resulted in the formation of a small well-mixed region with the higher fluid velocities around the Rushton impeller, while a large dead region was formed in the rest part of the stirred tank. On the contrary, as depicted in Fig. 11(b) and (c), when the SSO and DSO were employed with the same power consumption as the SSC, fluid flow was intensified in both axial and radial directions, and the well-mixed region increased significantly. The reason is that the impeller was closer to the wall. Compared with SSC at the same power consumption, the SSO and DSO agitated tanks have greater fluid velocity and flow range.

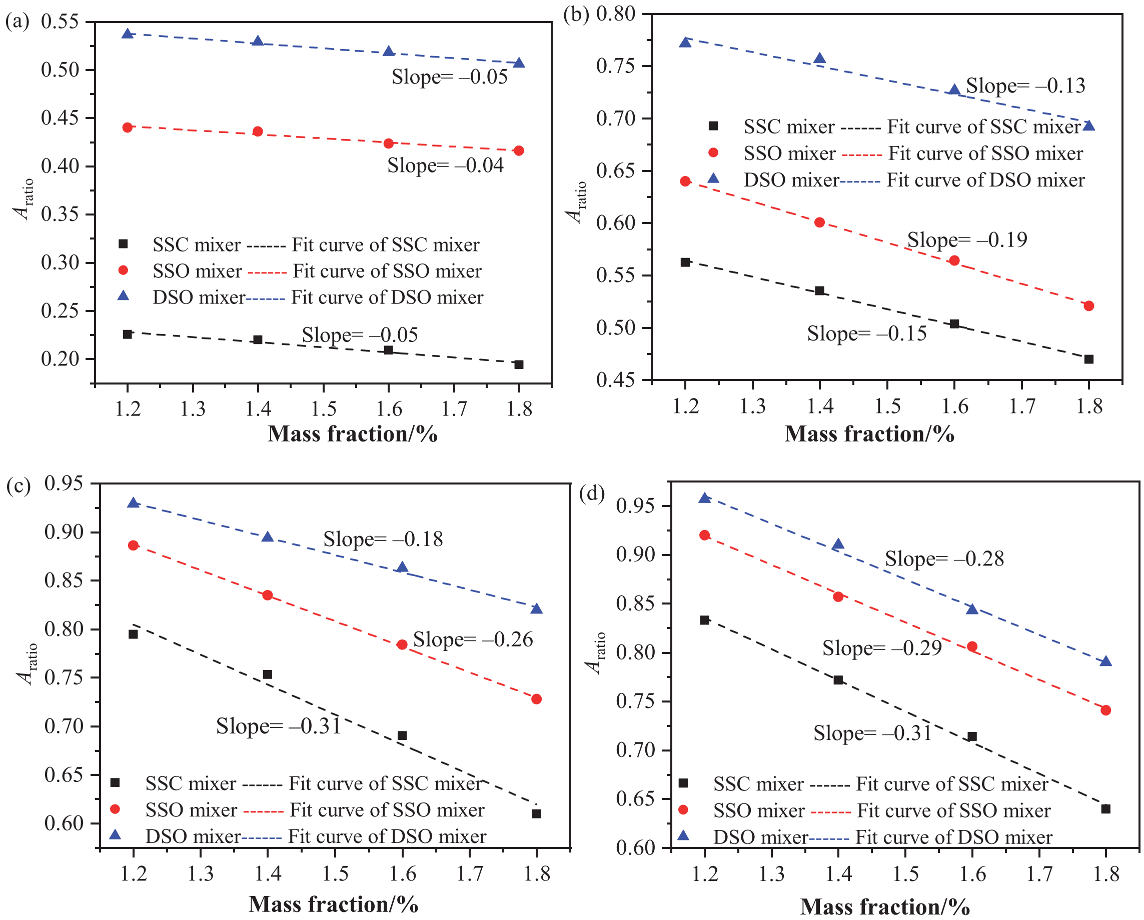

Fig. 9. The A_{ratio} variations of xanthan gum solutions as different mass fractions at different speed: (a) N = 120 r·min^{-1}, (b) N = 300 r·min^{-1}, (c) N = 480 r·min^{-1}, (d) N = 660 r·min^{-1}.

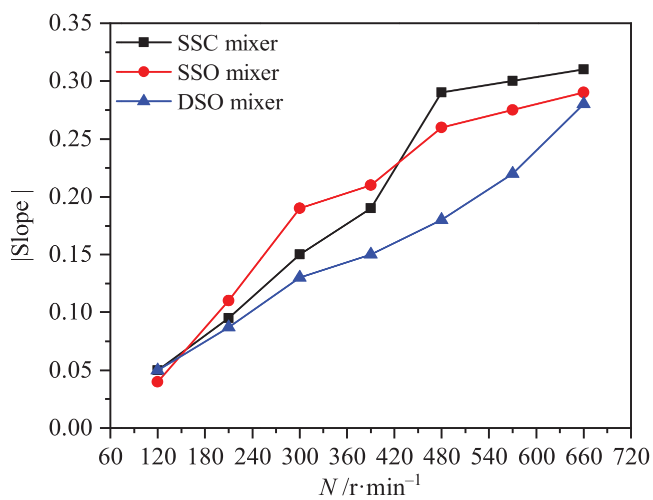

Fig. 10. The variation curves of the absolute value of slopes for three mixers at different speeds.

For further analysis, the 2D streamlines are plotted for the SSC, SSO and DSO mixers at the fixed power consumption of P = 5.7 W in Fig. 12. As presented in Fig. 12(a), the fluid flow generated by the SSC mainly occurred in the torus formed around the Rushton impeller. Four circulation loops were created around the two central Rushton impellers, and a symmetrical flow field structure was formed. It can be seen that the stagnant or slow-moving fluid areas occurred near the shaft and the upper part of the tank. For the SSO mixer, as shown in Fig. 12(b), the off-centred placed impellers broke the symmetrical flow field distribution in the tank, and intensified the axial flow of the fluid, especially the fluid between the stirred shaft and the wall near the shaft, while the fluid between the shaft and the wall farther away from shaft did not get the same axial strengthening effect. It can be noticed in Fig. 12(c) that the fluid flow created by the DSO was more abundant, and the streamlines were more evenly distributed. The reason may be that the dual-shaft agitation mode further disrupted the ordered structure of the flow field, and strengthened dynamic perturbations between two impellers in the tank. As a matter of fact, mixing achieved by using the DSO was more efficient than that for the SSC and the SSO. Comparison will be quantified later in this work with regard to the mixing time and mixing efficiency.

4.4. Mixing performance

4.4.1. Mixing time

The numerical simulations of the mixing procession are conducted through detecting the tracer concentration (taking water as a tracer in this work). The mixing time (t_{95}) can be obtained based on the 95% principle [42]. To compare the performances of three mixers in the mixing of the yield-pseudoplastic fluids, taking the xanthan gum solution with the mass fraction of 1.2% at N = 4 80 r·min^{-1} as an example, the tracer concentration response curves at four monitoring points are shown in Fig. 13. It can be seen that

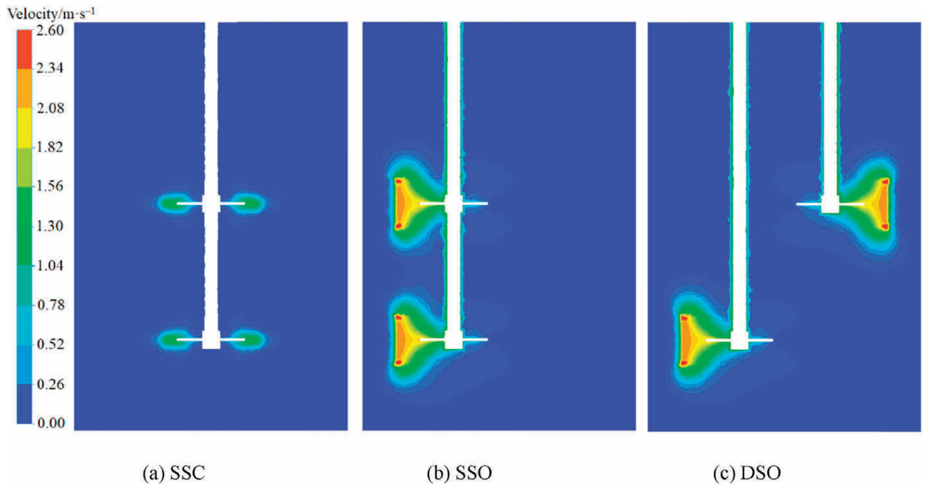

Fig. 11. Vertical velocity contour plots of the three mixers at P = 5.7 W and 1.2% xanthan gum solution.

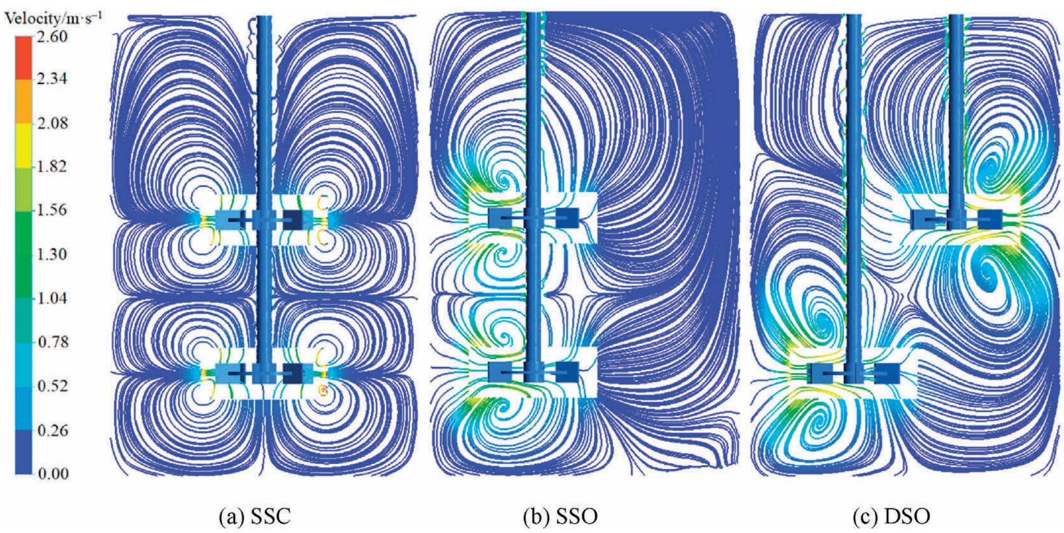

Fig. 12. The 2D streamlines of the three mixers at P = 5.7 W and 1.2% xanthan gum solution.

the concentration response curves of tracer fluctuate greatly at the beginning by rising sharply, and then it descends rapidly. Finally, it tends to be a straight line, which means the completion of the mixing process. The mixing time (t_{95}) of SSC, SSO and DSO was 8.31, 5.18 and 4.92 s, respectively.

It is necessary to compare the dimensionless mixing time (Nt_{95}) for three mixers at different Re^*. Fig. 14 shows the comparison of Nt_{95} for the three different mixing systems at different Reynolds numbers. As can be seen, the Nt_{95} unsurprisingly decreased linearly as an increase in the Re^*. At the same Re^*, the Nt_{95} of DSO was nearly 42.8% and 6.1% shorter than that of SSC and SSO, respectively. It indicated that DSO can shorten mixing time on the basis of same stirred condition, the advantages of DSO in terms of mixing rate were illustrated.

4.4.2. Mixing efficiency

Mixing rate reflects the time required to complete the mixing process, which is an important indicator that needs to be paid attention to in industrial production. At the same time, the power consumption of agitators is also a key factor to be considered. Hence, it is necessary to evaluate the mixing performance of single shaft central dual impellers, single shaft off-centred dual impellers and dual shaft off-centred impellers based on the specific power consumption.

The mixing efficiency is usually characterized by mixing energy per unit volume (W_v) and the power consumption per unit volume (P_v) [43,44], and the smaller the value of W_v, the higher the mixing efficiency. The W_v and P_v are defined as follows:

$$W_v = P_v t_{95} \quad (7)$$

$$P_v = \frac{2\pi NM}{V} \quad (8)$$

where V is the total volume of fluid in a stirred tank.

Fig. 15 shows the relationship between the mixing time (t_{95}) and P_v. As can be seen from Fig. 15, t_{95} decreases continuously as the increasing P_v, and t_{95} for SSO and DSO mixers are very close when P_v is higher than 2 kW·m^{-3}. At the same P_v, the t_{95} of DSO was shorter compared with that of SSC and SSO mixers. Therefore, DSO mixer could be recommended for the future in industrial production involving mixing of non-Newtonian fluids because of its shortest mixing time for the given power consumption.

The CFD results of torque and mixing energy per unit volume at different speeds are given in Table 3. The torque values are the sum

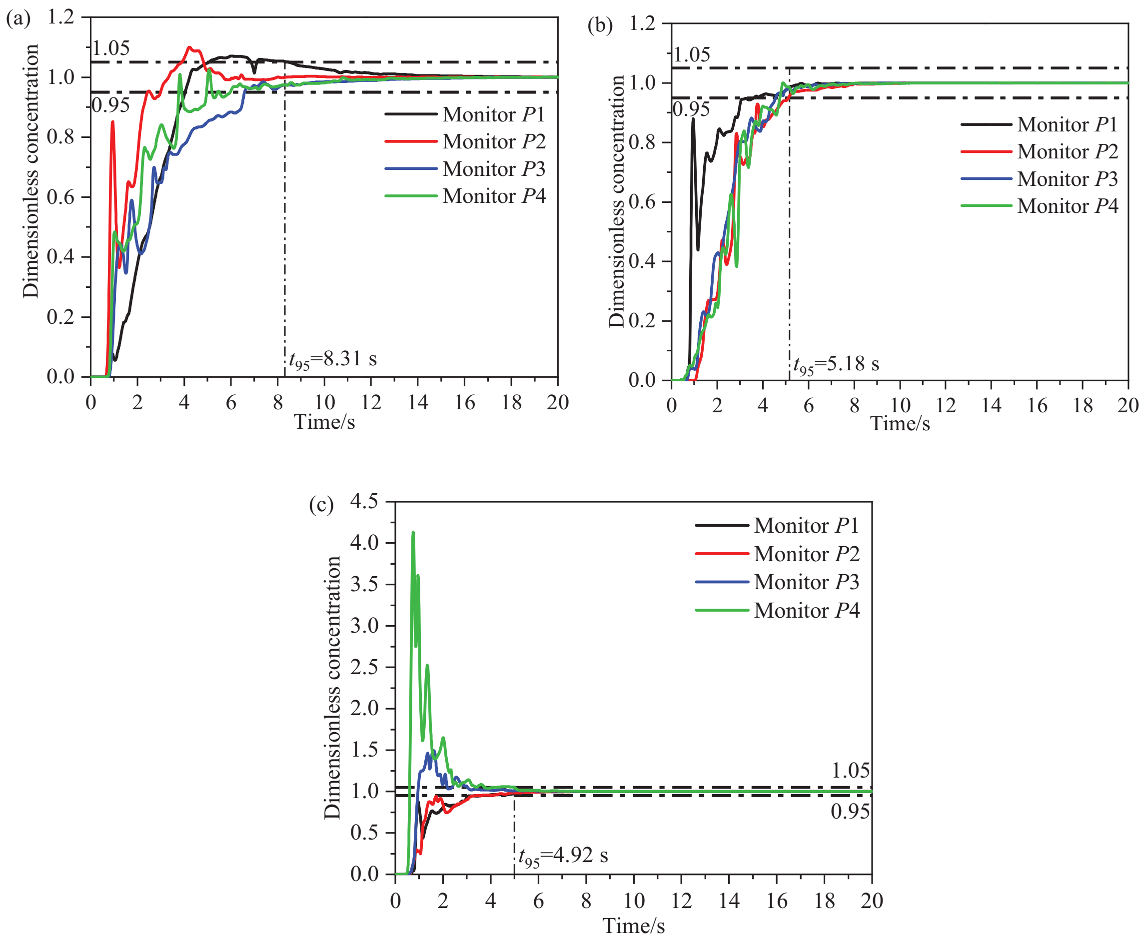

Fig. 13. Concentration response curve at different detecting points for three mixers: (a) SSC, (b) SSO, (c) DSO.

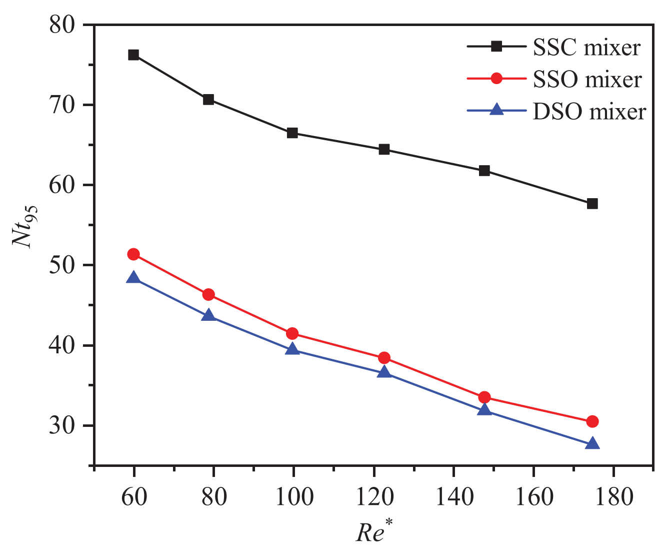

Fig. 14. The comparison of Nt_{95} for the three different mixing systems at different Reynolds numbers.

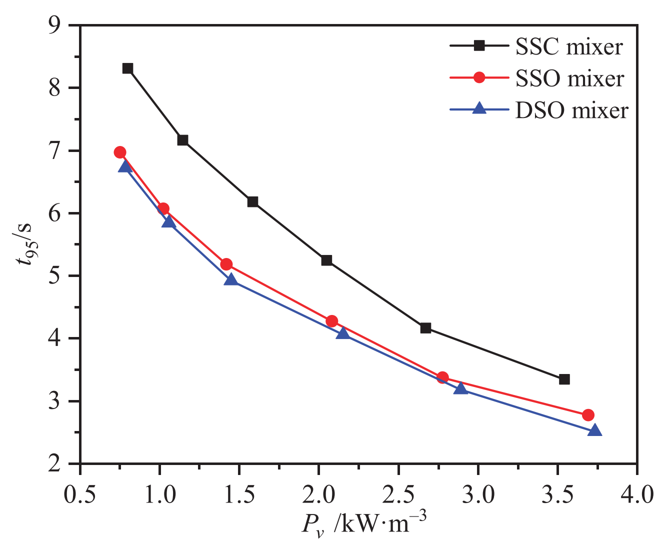

Fig. 15. Relationship between t_{95} and P_v for different mixers.

of each shaft and impeller under the corresponding stirring conditions.

It can be observed that the value of the mixing energy per unit volume of DSO was the smallest in the three stirred tanks at the same stirred speed, and the mixing energy per unit volume of DSO was 15.8% and 7.8% lower than that of SSC and SSO at N = 480 r·min^{-1}, respectively. As the rotational speed increased to 660 r·min^{-1}, the mixing energy per unit volume of DSO was 17.3% and 7.5% lower than that of SSC and SSO, respectively. These

Table 3
The calculation results of the torque and mixing energy per unit volume for the three stirred tanks at different speeds

N/r·min^{-1}	M /N·m			W_v /kJ·m^{-3}		
	SSC	SSO	DSO	SSC	SSO	DSO
480	0.26	0.46	0.47	7.82	7.14	6.58
540	0.33	0.60	0.62	8.95	8.24	7.66
600	0.41	0.72	0.75	10.28	9.36	8.74
660	0.49	0.86	0.88	11.54	10.31	9.54

results confirm our previous finding that the DSO was more effective than the SSC and SSO in the mixing of the yield-pseudoplastic fluids.

5. Conclusions

The hydrodynamic performance of the dual shaft off-centred mixer was assessed and compared to that of the single shaft central mixer and single shaft off-centred mixer with regards to the power consumption, generated flow domain, mixing time and mixing efficiency by using the torque test and CFD. Meanwhile, the influences of the fluid rheology and rotational speed on the development of cavern in a stirred tank with three impeller arrangements were also made an exploration deeply. The conclusions are obtained as follows:

The caverns of the three stirred tanks all developed from axial and radial direction as the increase of stirred speed, and the proportion of cavern in DSO mixer was better than that in SSC and SSO mixers at the same stirred condition. The fluid rheology has little influence on the variation of cavern area at the low speed (120 r·min^{-1}). When the A_{ratio} approached or reached its stable value, that is, the corresponding speed range from 480 to 660 r·min^{-1}, the A_{ratio} has a significant downward trend with the increase of the mass fraction of the fluid. The faster the rotating speed, the greater influence of the fluid rheology on the cavern area.

The dual-shaft agitation mode further disrupted the ordered structure of the flow field and strengthened dynamic perturbations between two impellers in the tank. Moreover, the mixing time t_{95} decreases continuously as the increasing P_v, and the Nt_{95} of DSO was nearly 42.8% and 6.1% shorter than that of SSC and SSO mixers at the same Re^*, respectively. The mixing energy per unit volume (W_v) of DSO was nearly 15.8% and 7.8% lower than that of SSC and SSO mixers at 480 r·min^{-1}, respectively. As the rotational speed increased to 660 r·min^{-1}, the W_v of DSO was 17.3% and 7.5% lower than that of SSC and SSO mixers. These results indicated that DSO mixer was more effective than SSC and SSO mixers in the mixing of the yield-pseudoplastic fluids.

Data Availability

Data will be made available on request.

Declaration of Competing Interest

The authors declare that they have no known competing financial interests or personal relationships that could have appeared to influence the work reported in this paper.

Acknowledgements

This work was supported by the National Natural Science Foundation of China (22078030, U1802255), National Key Research and Development Project (2019YFC1905802), Key Project of Independent Research Project of State Key Laboratory of Coal Mine Disaster Dynamics and Control (2011DA105287-zd201902), Three Gorges Laboratory Open Fund of Hubei Province (SK211009, SK215001).

Nomenclature

b	impeller blade width, m
C	off-bottom clearance, m
D	impeller diameter, m
D_d	disc diameter of impeller, m
d	shaft diameter, m
e	eccentric distance, m
H	fluid height, m
K	consistency index, Pa·s^n
k_s	constant of Metzner-Otto
L	spacing between two impellers, m
M	torque, N·m
N	impeller speed, r·s^{-1}
Nt_{95}	dimensionless mixing time
n	rheological index
P	power consumption
T	vessel diameter, m
t_{95}	mixing time, s
V	fluid volume, m^3
w	baffle width, m
w_t	mass fraction
$\dot{\gamma}$	shear rate, s^{-1}
η	non-Newtonian viscosity, Pa·s
ρ	density, kg·m^{-3}
τ	shear stress, Pa

References

[1] D.Y. Luan, S.J. Zhou, S.Y. Chen, S.P. Chu, CFD simulation of the flow field and cavern formation of pseudoplastic fluid with a 6-bent-blade impeller, *Chin. J. Process Eng.* 10 (6) (2010) 1054–1059. (in Chinese)
[2] D.Y. Luan, S.J. Zhou, S.Y. Chen, Cavern development of pseudoplastic fluids stirred by impeller of perturbed six-bent-bladed turbine, *J. Mech. Eng.* 48 (16) (2012) 1054–1059. (in Chinese)
[3] J.S. Ayala, H.L. de Moura, R. de Lima Amaral, F. de Assis Jr Oliveira, J.R. Nunhez, G.J. de Castilho, Two-dimensional shear rate field and flow structures of a pseudoplastic fluid in a stirred tank using particle image velocimetry, *Chem. Eng. Sci.* 248 (2022) 117198.
[4] Y.Y. Bao, B. Yang, Y. Xie, Z.M. Gao, Z.D. Zhang, T. Liu, X.H. Gao, Power demand and mixing performance of coaxial mixers in non-Newtonian fluids, *J. Chem. Eng. Japan* 44 (2) (2011) 57–66.
[5] S. Saeed, F. Ein-Mozaffari, S.R. Upreti, Using computational fluid dynamics to study the dynamic behavior of the continuous mixing of Herschel−Bulkley fluids, *Ind. Eng. Chem. Res.* 47 (19) (2008) 7465–7475.
[6] M. Zlokarnik, Stirring: Theory and Practice, Wiley-VCH, Weinhim, 2001.
[7] L. Pakzad, F. Ein-Mozaffari, P. Chan, Using electrical resistance tomography and computational fluid dynamics modeling to study the formation of cavern in the mixing of pseudoplastic fluids possessing yield stress, *Chem. Eng. Sci.* 63 (9) (2008) 2508–2522.
[8] P. Prajapati, F. Ein-Mozaffari, CFD investigation of the mixing of yield-pseudoplastic fluids with anchor impellers, *Chem. Eng. Technol.* 32 (8) (2009) 1211–1218.
[9] L. Rudolph, M. Schäfer, V. Atiemo-Obeng, M. Kraume, Experimental and numerical analysis of power consumption for mixing of high viscosity fluids with a co-axial mixer, *Chem. Eng. Res. Des.* 85 (5) (2007) 568–575.
[10] J. Sossa-Echeverria, F. Taghipour, Computational simulation of mixing flow of shear thinning non-Newtonian fluids with various impellers in a stirred tank, *Chem. Eng. Process. Process. Intensif.* 93 (2015) 66–78.

[11] C.W. Bakker, C.J. Meyer, D.A. Deglon, The development of a cavern model for mechanical flotation cells, *Miner. Eng.* 23 (11–13) (2010) 968–972.
[12] L. Pakzad, F. Ein-Mozaffari, S.R. Upreti, A. Lohi, A novel and energy-efficient coaxial mixer for agitation of non-Newtonian fluids possessing yield stress, *Chem. Eng. Sci.* 101 (2013) 642–654.
[13] F. Ein-Mozaffari, S.R. Upreti, Using ultrasonic Doppler velocimetry and CFD modeling to investigate the mixing of non-Newtonian fluids possessing yield stress, *Chem. Eng. Res. Des.* 87 (4) (2009) 515–523.
[14] L.W. Adams, M. Barigou, CFD analysis of caverns and pseudo-caverns developed during mixing of non-Newtonian fluids, *Chem. Eng. Res. Des.* 85 (5) (2007) 598–604.
[15] D.Y. Luan, Z.R. Wang, H. Wang, S.S. Wang, L.B. Li, Y.M. Chen, Determination method of the cavern boundary viscosity in a stirred tank with pseudoplastic fluid, *AIChE J.* 66 (5) (2020) e16941.
[16] J. Solomon, T.P. Elson, A.W. Nienow, G.W. Pace, Cavern sizes in agitated fluids with a yield stress, *Chem. Eng. Commun.* 11 (1–3) (1981) 143–164.
[17] T.P. Elson, D.J. Cheesman, A.W. Nienow, X-ray studies of cavern sizes and mixing performance with fluids possessing a yield stress, *Chem. Eng. Sci.* 41 (10) (1986) 2555–2562.
[18] A. Amanullah, S.A. Hjorth, A.W. Nienow, A new mathematical model to predict cavern diameters in highly shear thinning, power law liquids using axial flow impellers, *Chem. Eng. Sci.* 53 (3) (1998) 455–469.
[19] J. Sossa-Echeverria, F. Taghipour, Effect of mixer geometry and operating conditions on flow mixing of shear thinning fluids with yield stress, *AIChE J.* 60 (3) (2014) 1156–1167.
[20] L.K. Hui, C.P.J. Bennington, G.A. Dumont, Cavern formation in pulp suspensions using side-entering axial-flow impellers, *Chem. Eng. Sci.* 64 (3) (2009) 509–519.
[21] R.J. Wilkens, J.D. Miller, J.R. Plummer, D.C. Dietz, K.J. Myers, New techniques for measuring and modeling cavern dimensions in a Bingham plastic fluid, *Chem. Eng. Sci.* 60 (19) (2005) 5269–5275.
[22] Q. Xiao, N. Yang, J.H. Zhu, L.J. Guo, Modeling of cavern formation in yield stress fluids in stirred tanks, *AIChE J.* 60 (8) (2014) 3057–3070.
[23] D.Y. Luan, S.F. Zhang, J.P. Lu, X.G. Zhang, Chaotic characteristics enhanced by impeller of perturbed six-bent-bladed turbine in stirred tank, *Results Phys.* 7 (2017) 1524–1530.
[24] Z.H. Liu, X.Y. Yang, Z.M. Xie, R.L. Liu, C.Y. Tao, Y.D. Wang, Chaotic mixing performance of high-viscosity fluid synergistically intensified by flexible impeller and floating particles, *CIESC J. 64(8)* (2013) 2794–2800. (in Chinese)
[25] D.Y. Gu, Z.H. Liu, J. Li, Z.M. Xie, C.Y. Tao, Y.D. Wang, Intensification of chaotic mixing in a stirred tank with a punched rigid-flexible impeller and a chaotic motor, *Chem. Eng. Process. Process. Intensif.* 122 (2017) 2794–2800. (in Chinese)
[26] J. Aubin, C. Xuereb, Design of multiple impeller stirred tanks for the mixing of highly viscous fluids using CFD, *Chem. Eng. Sci.* 61 (9) (2006) 2913–2920.
[27] L. Pakzad, F. Ein-Mozaffari, S.R. Upreti, A. Lohi, Agitation of Herschel-Bulkley fluids with the Scaba-anchor coaxial mixers, *Chem. Eng. Res. Des.* 91 (5) (2013) 761–777.
[28] L. Pakzad, F. Ein-Mozaffari, S.R. Upreti, A. Lohi, Evaluation of the mixing of non-Newtonian biopolymer solutions in the reactors equipped with the coaxial mixers through tomography and CFD, *Chem. Eng. J.* 215–216 (2013) 279–296.
[29] L. Pakzad, F. Ein-Mozaffari, S.R. Upreti, A. Lohi, Using tomography to assess the efficiency of the coaxial mixers in agitation of yield-pseudoplastic fluids, *Chem. Eng. Res. Des.* 91 (9) (2013) 1715–1724.
[30] P.A. Tanguy, G. Ascanio, Mixing of shear-thinning fluids with dual off-centred impellers, *Can. J. Chem. Eng.* 83 (3) (2008) 393–400.
[31] F. Cabaret, C. Rivera, L. Fradette, M. Heniche, P.A. Tanguy, Hydrodynamics performance of a dual shaft mixer with viscous Newtonian liquids, *Chem. Eng. Res. Des.* 85 (5) (2007) 583–590.
[32] S. Saeed, F. Ein-Mozaffari, Using dynamic tests to study the continuous mixing of xanthan gum solutions, *J. Chem. Technol. Biotechnol.* 83 (4) (2008) 559–568.
[33] B. Letellier, C. Xuereb, P. Swaels, P. Hobbes, J. Bertrand, Scale-up in laminar and transient regimes of a multi-stage stirrer, A CFD approach, *Chem. Eng. Sci.* 57 (21) (2002) 4617–4632.
[34] A.B. Metzner, R.E. Otto, Agitation of non-Newtonian fluids, *AIChE J.* 3 (1) (1957) 3–10.
[35] H. Ameur, Effect of some parameters on the performance of anchor impellers for stirring shear-thinning fluids in a cylindrical vessel, *J. Hydrodyn. Ser B* 28 (4) (2016) 669–675.
[36] V. Buwa, A. Dewan, A.F. Nassar, F. Durst, Fluid dynamics and mixing of single-phase flow in a stirred vessel with a grid disc impeller: Experimental and numerical investigations, *Chem. Eng. Sci.* 61 (9) (2006) 2815–2822.
[37] D.Y. Gu, Z.H. Liu, Z.M. Xie, J. Li, C.Y. Tao, Y.D. Wang, Numerical simulation of solid–liquid suspension in a stirred tank with a dual punched rigid-flexible impeller, *Adv. Powder Technol.* 28 (10) (2017) 2723–2734.
[38] D.Y. Gu, C. Cheng, Z.H. Liu, Y.D. Wang, Numerical simulation of solid–liquid mixing characteristics in a stirred tank with fractal impellers, *Adv. Powder Technol.* 30 (10) (2019) 2126–2138.
[39] N.G. Deen, T. Solberg, B.H. Hjertager, Flow generated by an aerated Rushton impeller: Two-phase PIV experiments and numerical simulations, *Can. J. Chem. Eng.* 80 (4) (2008) 1–15.
[40] A. Brucato, M. Ciofalo, F. Grisafi, G. Micale, Numerical prediction of flow fields in baffled stirred vessels: A comparison of alternative modelling approaches, *Chem. Eng. Sci.* 53 (21) (1998) 3653–3684.
[41] A. Kazemzadeh, F. Ein-Mozaffari, A. Lohi, L. Pakzad, Investigation of hydrodynamic performances of coaxial mixers in agitation of yield-pseudoplasitc fluids: Single and double central impellers in combination with the anchor, *Chem. Eng. J.* 294 (2016) 417–430.
[42] Z. Jaworski, W. Bujalski, N. Otomo, A.W. Nienow, CFD study of homogenization with dual rushton turbines—Comparison with experimental results: Part I: Initial studies, *Chem. Eng. Res. Des.* 78 (3) (2000) 327–333.
[43] Q. Wu, X.X. Yan, X. Xia, C.Y. Zhang, T. Xue, K.C. Yu, P. Liang, X. Huang, Analysis of the mixing performance of a full-scale membrane bioreactor for municipal wastewater treatment, *Bioresour. Technol.* 250 (2018) 932–935.
[44] M.W.D. Brannock, Y. Wang, G. Leslie, Evaluation of full-scale membrane bioreactor mixing performance and the effect of membrane configuration, *J. Membr. Sci.* 350 (1–2) (2010) 101–108.